Radiation Effects on Dissipative Magnetohydrodynamic Couette Flow in a Composite Channel

Paresh Vyas[a] and Nupur Srivastava[b]

[a] Department of Mathematics, University of Rajasthan, Jaipur, 302004, India
[b] Department of Mathematics, Poornima University, Jaipur, 30395, India

Reprint requests to P. V.; E-mail: pvyasmaths@yahoo.com

Z. Naturforsch. **68a,** 554 – 566 (2013) / DOI: 10.5560/ZNA.2013-0038
Received July 18, 2012 / revised March 26, 2013 / published online July 3, 2013

This paper examines radiative thermal regime in dissipative magnetohydrodynamic (MHD) Couette flow in a composite parallel plate channel partially filled with a radiating fluid saturated porous medium and partially filled with a radiating clear fluid. The fluid is considered to be viscous, incompressible, optically dense, electrically conducting, and Newtonian. The radiative heat flux in the energy equation is assumed to follow the Rosseland approximation. Suitable matching conditions are used to match the momentum and thermal regimes in clear fluid and porous regions at the clear fluid–porous interface. The momentum and energy equations have closed form solutions. The effects of various parameters on the system are analyzed through graphs and tables.

Key words: Radiation; MHD Couette Flow; Composite Channel; Newtonian; Dissipation.

1. Introduction

Couette flow in parallel plate channel and associated heat transfer studies serve as good baby models in garnering pertinent 'core' first-hand information about many geophysical and industrial phenomenon. Though Couette flow is a classical problem in fluid mechanics but certainly, pressing needs of applications and the simple geometry have attracted investigators to revisit the problem with a variety of assumptions including Bhargava and Sancheti [1], Chauhan and Vyas [2], and many others. The Couette flow in parallel plate channels filled with a porous medium has also been studied by [3 – 7].

However, it has been experienced that though the porous medium enhances heat transfer but increases pressure drop too. To overcome this bottleneck, investigations were carried out in composite channels (Vafai and Kim [8], Huang and Vafai [9, 10]). Recently several works have been reported on the efficacy of porous substrate in heat transfer augmentation (Kaviany [11, 12], Nield and Kuznetsov [13], Hooman et al. [14], Baoku et al. [15]). The findings revealed that the channels partially filled with a porous medium can still be reasonably effective in heat transfer augmentation. The heat transfer studies in composite ducts were motivated by two major issues: firstly, the urging need to address the problem of heat transfer enhancement under the given constraints; secondly, there are areas such as geothermal engineering, industrial engineering etc. where one comes across the fluid–porous interface. The analysis of flow and thermal characteristics at the fluid–porous interface is of immense significance in numerous processes such as pollutant dispersion in aquifers, environment transport processes, separation processes in chemical industry, flow past porous scaffolds in bioreactors, drying process, ceramic processing etc.

Thus, prompted by the numerous applications cutting across different realms, investigations of flow and heat transfer in composite channels have been reported (Sahraoui and Kaviany [16], Kuznetsov [17 – 19], Alkam et al. [20], Al-Nimr and Khadrawi [21], Chauhan and Rastogi [22, 23], Komurgoz et al. [24], Chauhan and Agrawal [25, 26], Kaurangini and Jha [27]). It is pertinent to mention that the composite channel studies have grown considerably due to much headway in proper conditions matching the velocity and/or temperature of the clear fluid region and that of the porous region at the interface (Beavers and Joseph [28], Neale and Nader [29], Kim and Russell [30], Vafai and Thiyagaraja [31]). Here, we are inclined to clarify that the issue of boundary conditions at the clear fluid–porous interface is still open. Some

authors are reluctant to appreciate the idea of continuity of shear stress across the clear fluid–porous interface and advocate the continuity of velocity only across the clear fluid–porous interface but not that of shear stress (Ochoa-Tapia and Whitakar [32, 33], who observed a jump in the shear stress at the interface). Here it should be noted that given to complex structures of porous materials these conditions were derived under certain assumptions. Hence, there is still a general understanding that different porous media have distinct structure characteristics and therefore may warrant interface conditions accordingly. In this regard, fabulous survey and analysis pertaining to the different matching conditions at the clear fluid–porous interface (Alazmi and Vafai [34]) is worth to take note of, who examined the effects of various conditions at the interface on the velocity and temperature fields. They found substantial results that though the velocity field was sensitive to the different matching conditions at the fluid–porous interface but there was no substantial quantitative difference in the temperature field for different matching conditions. They concluded that there were at the most 2% variations in the thermal quantities of interest for different interfacial conditions. In view of the above discussion, in order to analyze radiative thermal regime in composite channel, we felt free to follow the conditions suggested by Kim and Russell [30] that indicate continuity in velocity and shear as well besides continuity in temperature and temperature gradient across the interface.

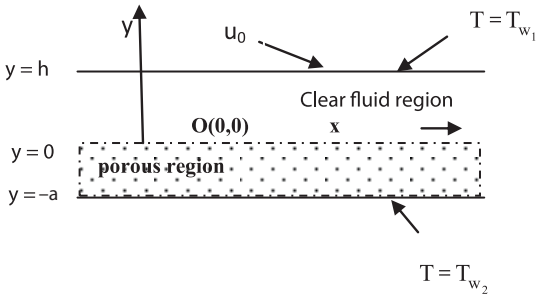

Fig. 1. Schematic Diagram.

Thermal studies with dissipation aspects are significant in devising optimal systems. It is pertinent to record that dissipation is observed to be quantitatively inferior as compared to its other counterpart effects but certainly has appreciable qualitative effects. One may recall that viscous dissipation physically means the local production of thermal energy due to viscous stresses. The effect is encountered in both the viscous flow of clear fluids and the fluid flow through the porous medium. A great deal of discussion on the expressions envisaging dissipation in porous media is available in the literature. The dissipation φ in porous region is assumed to take the following form (A. K. Al-Hadhrami et al. [35]):

$$\varphi = \bar{\mu}\left(\frac{\mathrm{d}u}{\mathrm{d}y}\right)^2 + \frac{\mu}{k}u^2.$$

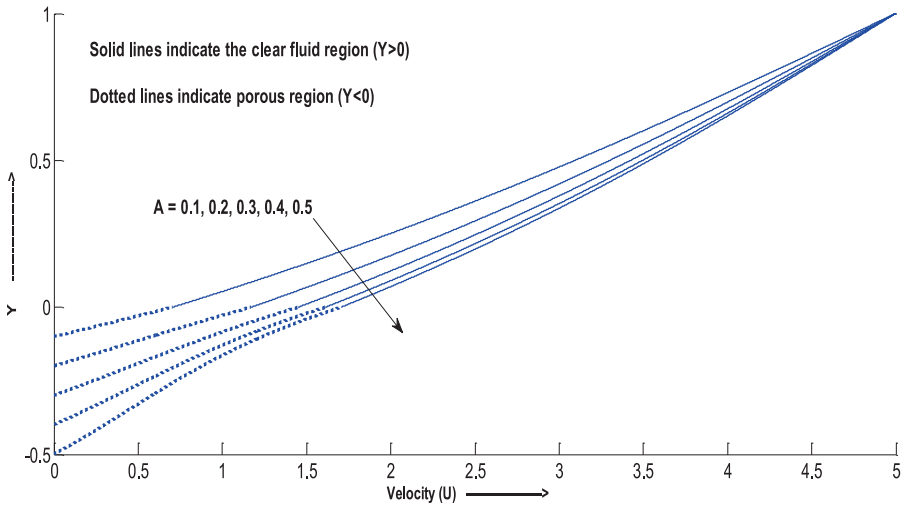

Fig. 2 (colour online). Velocity distribution for variation in A when $M = 1$, $K_0 = 0.1$, $C_1 = 5$, $\varphi_1 = 0.8$, and $U_0 = 5$.

Radiative heat transfer studies are important in the thermal regimes involving high temperatures. Though, radiative studies are complex and cumbersome due to the intricacies involved, but thankfully, some reasonable simplifications have been found to work satisfactorily. Many authors have conducted radiative heat transfer studies in flow configuration with and without a porous medium (Plumb et al. [36], Vyas and Srivastava [37 – 39], Vyas and Ranjan [40], Vyas and Rai [41, 42], Pop et al. [43], Hayat et al. [44]).

To the best of the knowledge to the authors', radiation effects in composite duct flow have not been reported. This motivated us to carry out the presented work. It is expected that the model presented here would serve as a pertinent introductory analysis for further explorations.

2. Mathematical Model and Solution

Let us consider the magnetohydrodynamic (MHD) radiative flow of a viscous electrically conducting incompressible fluid between two horizontal walls at a distance h apart (Fig. 1). The upper wall is rigid and moving with a uniform velocity u_0 whilst the lower wall is a stationary porous bed of finite thickness a with an impermeable bottom. A Cartesian coordinate system is used where O_{xyz} constitutes a set of orthogonal axes with origin at the interface. The walls are parallel to the x,z-plane. The channel is very long and is of large width in the z-direction.

The flow regime is divided into two zones: I – the clear fluid region ($0 \le y \le h$), II – the porous region ($-a \le y \le 0$). The flow is caused by applying a constant pressure gradient $\partial p/\partial x$ at the mouth of the channel and due to the movement of the upper wall. The upper wall and the bottom of the porous bed bear constant temperature T_{w_1} and T_{w_2}, respectively ($T_{w_1} > T_{w_2}$). A uniform magnetic field of strength B_0 is applied parallel to the y-axis. The induced magnetic field is neglected, which is valid for small magnetic Reynolds number. The radiative flux in the energy equation is described by the Roseland approximation which simulates radiation in optically thick fluids reasonably well wherein thermal radiation travels a short distance before being scattered or absorbed.

The following assumptions are also made in the investigations:

i. The flow is steady, laminar, and fully developed.
ii. The fluid is absorbing–emitting radiations but it is non-scattering.
iii. The plates are perfect insulators.
iv. The fluid is assumed to be Newtonian and without phase change.
v. The fluid and the porous medium are in local thermal equilibrium.

Under these conditions, considering the Brinkman model for the porous medium, the governing equations for the setup under consideration are

Region I ($0 \le y \le h$):

$$\mu \frac{\mathrm{d}^2 u_1}{\mathrm{d}y^2} - \sigma B_0^2 u_1 = \frac{\partial p}{\partial x}, \tag{1}$$

$$\kappa \frac{\mathrm{d}^2 T_1}{\mathrm{d}y^2} + \mu \left(\frac{\mathrm{d}u_1}{\mathrm{d}y}\right)^2 - \frac{\partial q_\mathrm{r}}{\partial y} = 0. \tag{2}$$

Region II ($-a \le y \le 0$):

$$\bar{\mu} \frac{\mathrm{d}^2 u_2}{\mathrm{d}y^2} - \sigma B_0^2 u_2 - \frac{\mu}{k_0} u_2 = \frac{\partial p}{\partial x}, \tag{3}$$

$$\bar{\kappa} \frac{\mathrm{d}^2 T_2}{\mathrm{d}y^2} + \bar{\mu} \left(\frac{\mathrm{d}u_2}{\mathrm{d}y}\right)^2 + \frac{\mu}{k_0} u_2^2 - \frac{\partial q_\mathrm{r}}{\partial y} = 0. \tag{4}$$

Here the subscripts 1 and 2 denote the quantities for Region I and Region II respectively.

The quantities u, p, κ, μ, υ, T, q_r, k_0, and σ denote the fluid velocity, pressure, thermal conductivity, coefficient of viscosity, kinematic viscosity, temperature, radiative heat flux, permeability, and electrical conductivity, respectively. The quantities $\bar{\mu}$ and $\bar{\kappa}$ are effective viscosity and effective thermal conductivity, respectively, of the porous medium.

The boundary and interface conditions on velocity and temperature are

$$\begin{aligned}
&y = h: \;\; u_1 = u_0, \;\; T = T_{w_1}, \\
&y = 0: \;\; u_1 = u_2, \;\; \left(\mu \frac{\mathrm{d}u_1}{\mathrm{d}y}\right) = \left(\bar{\mu} \frac{\mathrm{d}u_2}{\mathrm{d}y}\right), \\
&\text{and} \;\; T_1 = T_2, \;\; \left(\kappa \frac{\mathrm{d}T_1}{\mathrm{d}y}\right) = \left(\bar{\kappa} \frac{\mathrm{d}T_2}{\mathrm{d}y}\right), \\
&y = -a: \;\; u_2 = 0, \;\; T = T_{w_2}.
\end{aligned} \tag{5}$$

We assume that $\partial p/\partial x = -C$ (constant).

The radiation heat flux q_r in the energy equation is assumed to follow the Rosseland approximation (Brewster [45], Modest [46]) and is given as

$$q_r = -\frac{4\sigma^*}{3k^*}\frac{\partial T^4}{\partial y}, \tag{6}$$

where σ^* and k^* are the Stephan–Boltzmann constant and mean absorption constant, respectively. We assume that the temperature difference within the fluid is sufficiently small so that T^4 may be expressed as a linear function of the temperature T. This is done by expanding T^4 in a Taylor series about T_{w_2} and omitting higher-order terms to yield

$$T^4 \cong 4T_{w_2}^3 T - 3T_{w_2}^4. \tag{7}$$

3. Method of Solution

We now introduce the following non-dimensional quantities:

$$\begin{aligned} &X = \frac{x}{h},\ Y = \frac{y}{h},\ U = \frac{uh}{\upsilon},\ P = \frac{ph^2}{\rho\upsilon^2}, \\ &A = \frac{a}{h},\ K_0 = \frac{k_0}{h^2},\ \theta = \frac{T - T_{w_2}}{T_{w_1} - T_{w_2}}. \end{aligned} \tag{8}$$

In view of (8), the governing equations (1) through (4) take the following non-dimensional forms:

Region I $(0 \le Y \le 1)$*:*

$$\frac{d^2U_1}{dY^2} - M^2U_1 = -C_1, \tag{9}$$

$$\frac{d^2\theta_1}{dY^2} = \frac{-\mathrm{Br}}{(1+4\mathrm{Nr}/3)}\left(\frac{dU_1}{dY}\right)^2. \tag{10}$$

Region II $(-A \le Y \le 0)$*:*

$$\frac{d^2U_2}{dY^2} - N^2U_2 = -\frac{C_1}{\varphi_1}, \tag{11}$$

$$\frac{d^2\theta_2}{dY^2} = \frac{-\mathrm{Br}}{\varphi_2(1+4\mathrm{Nr}/3\varphi_2)}\left[\varphi_1\left(\frac{dU_2}{dY}\right)^2 + \frac{U_2^2}{K_0}\right]. \tag{12}$$

And the boundary conditions (5) in non-dimensional form are reduced to

$$\begin{aligned} &Y = 1:\ U_1 = U_0,\ \theta_1 = 1, \\ &Y = 0:\ U_1 = U_2,\ \frac{dU_1}{dY} = \varphi_1\frac{dU_2}{dY}, \\ &\qquad \theta_1 = \theta_2,\ \frac{d\theta_1}{dY} = \varphi_2\frac{d\theta_2}{dY}, \\ &Y = -A:\ U_2 = 0,\ \theta_2 = 0, \end{aligned} \tag{13}$$

where $M = \sqrt{\frac{h^2\sigma B_0^2}{\mu}}$, $\mathrm{Nr} = \frac{4\sigma^* T_{w_2}^3}{k^*\kappa}$, and $\mathrm{Br} = \frac{\mu\upsilon^2}{\kappa h^2(T_{w_1} - T_{w_2})}$ are Hartmann parameter, radiation parameter, and Brinkman number, respectively. Also $U_0 = \frac{u_0 h}{\upsilon}$, $\frac{\partial P}{\partial X} = -C_1$, $N^2 = \frac{1}{\varphi_1}\left(M^2 + \frac{1}{K_0}\right)$, $\varphi_1 = \frac{\bar{\mu}}{\mu}$, and $\varphi_2 = \frac{\bar{\kappa}}{\kappa}$.

The equations for velocity and temperature fields for both the regions given in (9) through (12) are linear ordinary differential equations hence are amenable to closed form analytical solutions. Solving (9) through (12), we get the solutions as

Region I $(0 \le Y \le 1)$*:*

$$U_1 = A_1 e^{MY} + B_1 e^{-MY} + \frac{C_1}{M^2}, \tag{14}$$

$$\begin{aligned} \theta_1 = &-\frac{\mathrm{Br}}{4(1+4\mathrm{Nr}/3)}\left(A_1^2 e^{2MY} + B_1^2 e^{-2MY}\right. \\ &\left. - 4A_1B_1M^2Y^2\right) + D_1Y + D_2. \end{aligned} \tag{15}$$

Region II $(-A \le y \le 0)$*:*

$$U_2 = A_2 e^{NY} + B_2 e^{-NY} + \frac{C_1}{\varphi_1 N^2}, \tag{16}$$

$$\begin{aligned} \theta_2 = &D_3Y + D_4 - \frac{\mathrm{Br}}{\varphi_2(1+4\mathrm{Nr}/3\varphi_2)}\left[\varphi_1\left(1+\frac{1}{\varphi_1K_0N^2}\right)\right. \\ &\cdot\left(\frac{A_2^2}{4}e^{2NY} + \frac{B_2^2}{4}e^{-2NY}\right) + \frac{C_1^2Y^2}{2\varphi_1^2K_0N^4} + \frac{2C_1}{\varphi_1K_0N^4} \\ &\left.\cdot\left(A_2e^{NY} + B_2e^{-NY}\right) - A_2B_2N^2\left(\varphi_1 - \frac{1}{K_0N^2}\right)Y^2\right], \end{aligned} \tag{17}$$

where A_1, B_1, D_1, D_2, A_2, B_2, D_3, and D_4 are constants of integration to be evaluated in view of (13). We apply the boundary conditions given by (13) to (14) and (16) and obtain the simultaneous equations in A_1, A_2, B_1, B_2 as

$$A_1e^{M} + B_1e^{-M} = U_0 - \frac{C_1}{M^2}, \tag{18}$$

$$A_1 - A_2 + B_1 - B_2 = C_1\left(\frac{1}{\varphi_1N^2} - \frac{1}{M^2}\right), \tag{19}$$

$$MA_1 - \varphi_1NA_2 - MB_1 + \varphi_1NB_2 = 0, \tag{20}$$

$$A_2e^{-AN} + B_2e^{AN} = -\frac{C_1}{\varphi_1N^2}. \tag{21}$$

We now apply boundary conditions given by (13) to (15) and (17) to get the simultaneous equations in D_1, D_2, D_3, D_4 as

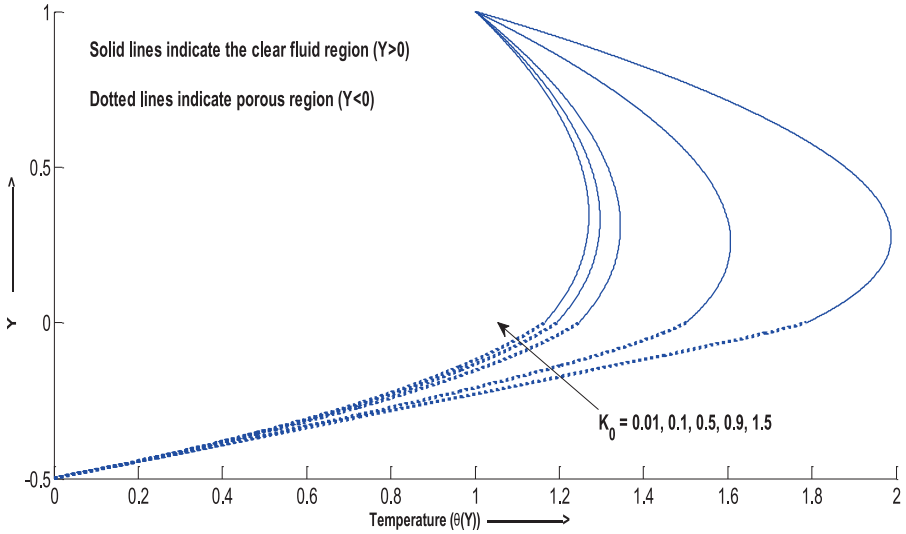

Fig. 3 (colour online). Temperature distribution for varying values of K_0 when $M = 1$, $A = 0.5$, $C_1 = 5$, $U_0 = 5$, $\mathrm{Br} = 0.5$, $\mathrm{Nr} = 1$, $\varphi_1 = 0.8$, and $\varphi_2 = 0.6$.

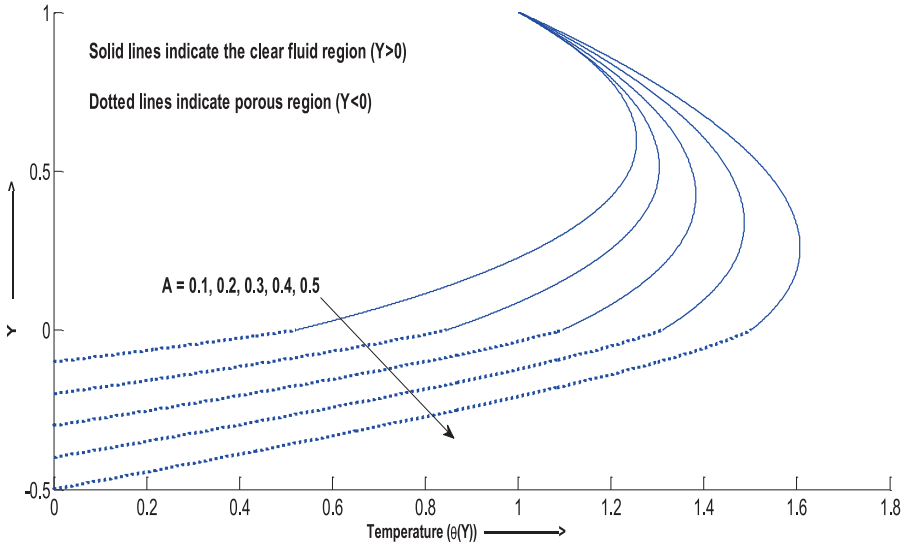

Fig. 4 (colour online). Temperature distribution for varying thickness A of the porous layer when $M = 1$, $K_0 = 0.1$, $C_1 = 5$, $U_0 = 5$, $\mathrm{Br} = 0.5$, $\mathrm{Nr} = 1$, $\varphi_1 = 0.8$, and $\varphi_2 = 0.6$.

$$D_1 + D_2 = 1 + \frac{\mathrm{Br}}{4(1+4\mathrm{Nr}/3)}\left(A_1^2 \mathrm{e}^{2M} + B_1^2 \mathrm{e}^{-2M} - 4M^2 A_1 B_1\right), \tag{22}$$

$$D_2 - D_4 = \frac{-\mathrm{Br}}{\varphi_2(1+4\mathrm{Nr}/3\varphi_2)}\left[\frac{2C_1(A_2+B_2)}{\varphi_1 K_0 N^4} + \frac{\varphi_1}{4} \cdot \left(1+\frac{1}{\varphi_1 K_0 N^2}\right)\left(A_2^2+B_2^2\right)\right] + \frac{\mathrm{Br}\left(A_1^2+B_1^2\right)}{4(1+4\mathrm{Nr}/3)}, \tag{23}$$

$$D_1 - \varphi_2 D_3 = \frac{-\mathrm{Br}}{(1+4\mathrm{Nr}/3\varphi_2)}\left[\frac{N\varphi_1}{2}\left(1+\frac{1}{\varphi_1 K_0 N^2}\right)\left(A_2^2 - B_2^2\right) + \frac{2C_1 N(A_2 - B_2)}{\varphi_1 K_0 N^4}\right] + \frac{M\mathrm{Br}\left(A_1^2 - B_1^2\right)}{2(1+4\mathrm{Nr}/3)}, \tag{24}$$

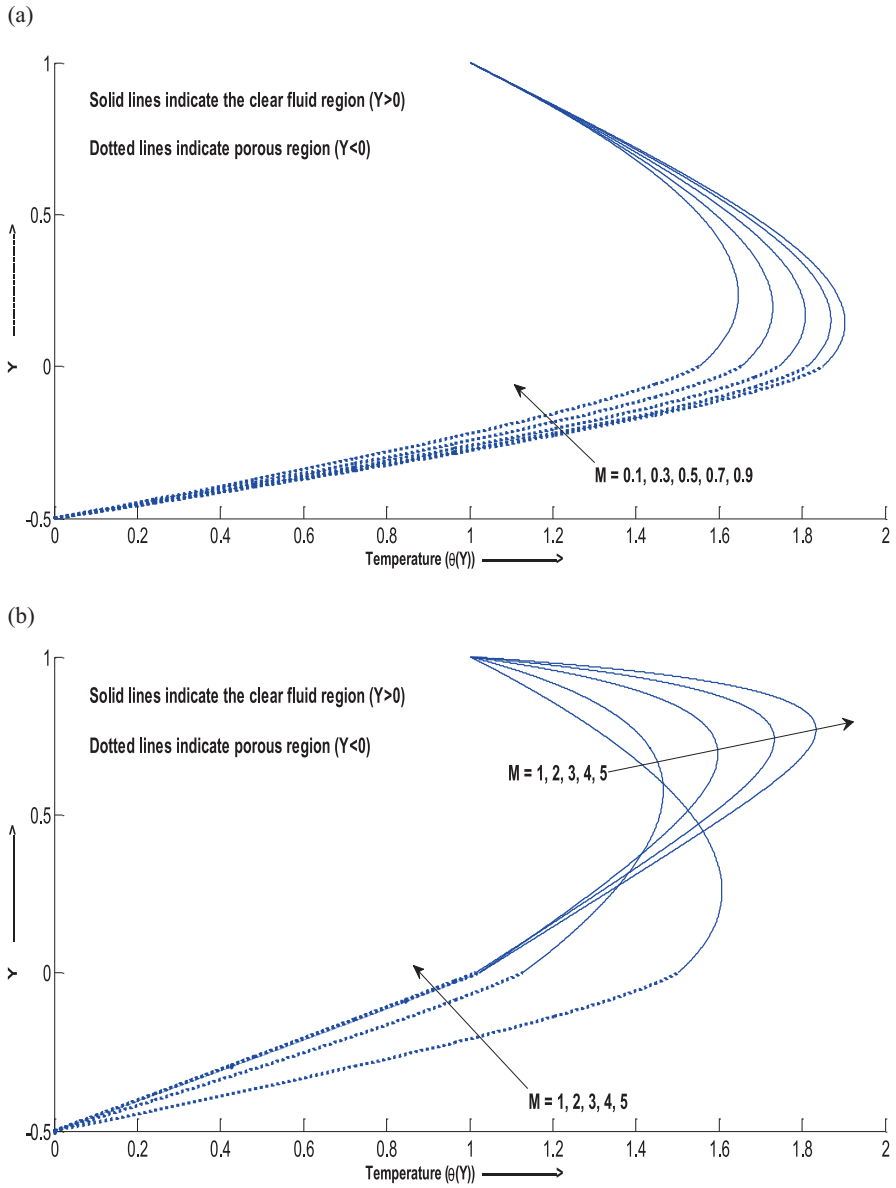

Fig. 5 (colour online). (a) Temperature distribution for variation in M ($M < 1$) when $K_0 = 0.1$, $A = 0.5$, $C_1 = 5$, $U_0 = 5$, $\mathrm{Br} = 0.5$, $\mathrm{Nr} = 1$, $\varphi_1 = 0.8$, and $\varphi_2 = 0.6$. (b) Temperature distribution for variation in M ($M \geq 1$), when $K_0 = 0.1$, $A = 0.5$, $C_1 = 5$, $U_0 = 5$, $\mathrm{Br} = 0.5$, $\mathrm{Nr} = 1$, $\varphi_1 = 0.8$, and $\varphi_2 = 0.6$.

$$AD_3 - D_4 = \frac{-\mathrm{Br}}{\varphi_2(1+4\mathrm{Nr}/3\varphi_2)}\left[\frac{\varphi_1}{4}\left(1+\frac{1}{\varphi_1 K_0 N^2}\right)\right.$$
$$\left(A_2^2\,\mathrm{e}^{-2AN} + B_2^2\,\mathrm{e}^{2AN}\right) + \frac{2C_1\left(A_2\,\mathrm{e}^{-AN} + B_2\,\mathrm{e}^{AN}\right)}{\varphi_1 K_0 N^4} \quad (25)$$
$$\left. + \frac{C_1^2 A^2}{2\varphi_1^2 K_0 N^4} - A_2 B_2 A^2 N^2\left(\varphi_1 - \frac{1}{K_0 N^2}\right)\right].$$

The system of linear equations (18) through (21) and (22) through (25) for the unknowns A_1, A_2, B_1, B_2, D_1, D_2, D_3, and D_4 have been solved by MATLAB using the module LINSOLVE. Thus the complete solution of (14) through (17) is obtained numerically.

In order to get an insight of the phenomena under study, we have drawn the profiles for velocity and tem-

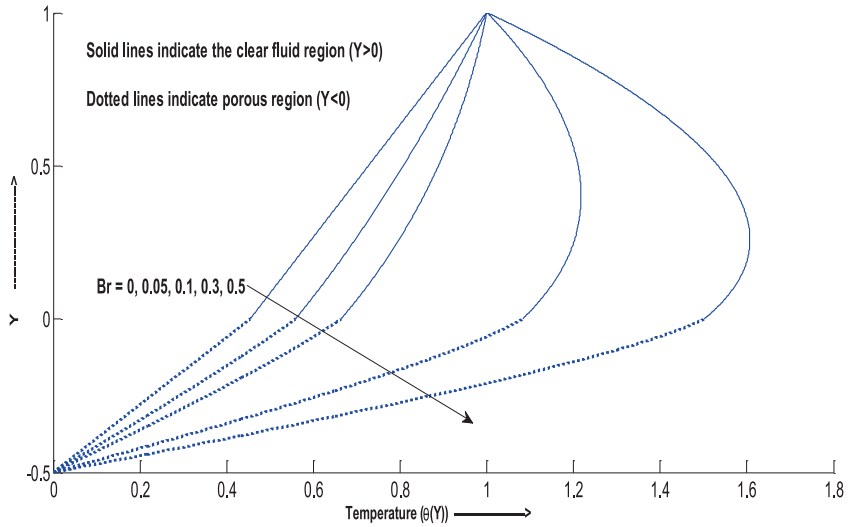

Fig. 6 (colour online). Temperature distribution for varying values of Br when $M = 1$, $K_0 = 0.1$, $C_1 = 5$, $U_0 = 5$, $A = 0.5$, $\mathrm{Nr} = 1$, $\varphi_1 = 0.8$, and $\varphi_2 = 0.6$.

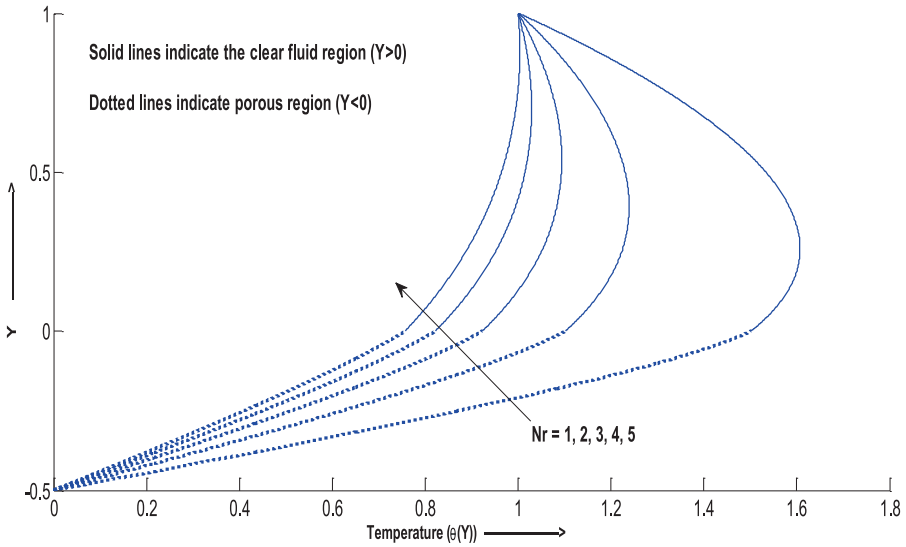

Fig. 7 (colour online). Temperature distribution for varying values of Nr when $M = 1$, $K_0 = 0.1$, $C_1 = 5$, $U_0 = 5$, $A = 0.5$, $\mathrm{Br} = 0.5$, $\varphi_1 = 0.8$, and $\varphi_2 = 0.6$.

perature distributions and rates of heat transfer at the upper wall and at the bottom of the porous bed. The critical Brinkman number $\mathrm{C_{Br}}$ at the upper wall is also computed and is shown in a tabular form.

4. Results and Discussions

In order to peep into the phenomenon, the profiles for velocity distribution, temperature distribution, and rates of heat transfer at the walls have been drawn and are discussed here. It is to be noted that in the velocity and temperature profiles, the dotted lines ($-0.5 \leq Y \leq 0$) indicate the porous region and the solid lines ($0 \leq Y \leq 1$) indicate the clear fluid region. Figure 2 exhibits the effect of thickness A of the porous layer on the velocity distribution. The figure reveals that the velocity increases with an increase in A. This finding is significant in designing of engineering devices where higher velocity can be obtained with the insertion of a porous layer.

Table 1. Variation of C_{Br} with respect to U_0 and M when $K_0 = 0.1$, $C_1 = 5$, $A = 0.5$, Nr $= 1$, $\varphi_1 = 0.8$, and $\varphi_2 = 0.6$.

$U_0 = 1$		$U_0 = 5$	
M	C_{Br}	M	C_{Br}
0.1	0.57090	0.1	0.14504
0.6	0.70540	0.6	0.14649
1.0	1.02080	1.0	0.13802
2.0	3.65600	2.0	0.07990
2.6	3.91470	2.6	0.05582
3.0	2.8751	3.0	0.04562
4.0	1.34880	4.0	0.03090

Table 2. Variation of C_{Br} with respect to U_0 and K_0 when $C_1 = 5$, $A = 0.5$, Nr $= 1$, $\varphi_1 = 0.8$, and $\varphi_2 = 0.6$; for the cases when Hartmann number $M = 0.5$, 1.0, and 2.0.

$U_0 = 1$			$U_0 = 5$		
M	K_0	C_{Br}	M	K_0	C_{Br}
	0.1	0.66050		0.1	0.14663
0.5	0.5	0.55061	0.5	0.5	0.21535
	1.0	0.50500		1.0	0.91200
	0.1	1.02080		0.1	0.13802
1.0	0.5	0.94900	1.0	0.5	0.19144
	1.0	0.91200		1.0	0.20519
	0.1	3.6560		0.1	0.07990
2.0	0.5	5.4140	2.0	0.5	0.08688
	1.0	5.8990		1.0	0.08823

Table 3. Variation in C_{Br} with respect to U_0, A, and Nr when $M = 1$, $K_0 = 0.1$, $C_1 = 5$, $\varphi_1 = 0.8$, and $\varphi_2 = 0.6$.

$U_0 = 1$			$U_0 = 5$		
A	Nr	C_{Br}	A	Nr	C_{Br}
0.1	1.0	3.08540	0.1	1.0	0.20624
0.3	1.0	1.63000	0.3	1.0	0.17623
0.5	1.0	1.02080	0.5	1.0	0.13802
0.5	2.0	1.64500	0.5	2.0	0.21960
0.5	3.0	2.26900	0.5	3.0	0.30110
0.5	4.0	2.89180	0.5	4.0	0.38248

Figure 3 displays the variation in temperature θ for varying values of permeability parameter K_0. It is revealed that the temperature decays with increasing values of the permeability parameter. The porous layer offers low impedance to the fluid traversal inside for higher values of K_0. This indicates a rather shorter cooling time by having larger values of K_0.

Figure 4 displays the variation in temperature θ for varying values of thickness A of the porous layer. The figure reveals that there is a substantial increase in temperature for increasing values of A. This finding is of immense importance in devices having porous strips and underlines the utility of a porous medium in heat transfer augmentation.

The effect of Hartmann number (magnetic field parameter) M on the temperature field has been shown in Figures 5a and b. The effect of the Hartmann number has been analyzed for the two cases $M < 1$ (Fig. 5a) and $M \geq 1$ (Fig. 5b). Figure 5a reveals that the temperature decreases uniformly in the whole region with an increase in the values of M (< 1). Figure 5b displays the case when the values of M are higher than 1. In this case the effect of M is somewhat abnormal. As it is evident from the very figure, we find that in the upper region adjacent to the upper wall, the temperature rises consistently with the increasing values of M and has a parabolic distribution. However, in the lower middle clear-fluid region, the temperature distribution is somewhat peculiar for $M = 1$ and $M = 2$. In contrast to this, the temperature in the porous region and its vicinity decays consistently with increasing values of M.

Figure 6 depicts the variation in temperature for varying values of Brinkman number Br. The figure reveals that the temperature θ registers increment with the increasing values of Br in both clear fluid and porous regions. In fact, we note that for a given value of the temperature difference $T_{w_1} - T_{w_2} > 0$ heat flows from the upper plate to the fluid as long as Br does not exceed a certain value, after that the maximum temperature shifts from the upper wall region to mid plane and heat flows from the fluid to the upper wall. Larger values of the Brinkman number are indicative of rather more frictional heating in the system thereby causing a rise in the temperature. In fact, frictional heating serves as energy source to modify the thermal regime.

Figure 7 displays the variation in temperature θ for varying values of the radiation parameter Nr. The effect of higher values of Nr is to decrease θ.

The rates of heat transfer at the plates for different values of the parameters involved have been displayed in Figures 8 – 11. It is to be noted that in these figures the rate of heat transfer is calculated at the impermeable bottom of the stationary porous bed (indicated by dotted lines) and at the moving upper wall (indicated the solid lines).

Figure 8 displays rates of heat transfer at the upper wall and at the impermeable bottom for varying values of the permeability parameter. From the very figure we conclude that the temperature gradient $\mathrm{d}\theta/\mathrm{d}Y$ at the upper plate reduces numerically while it increases at the bottom of the porous layer with increasing values

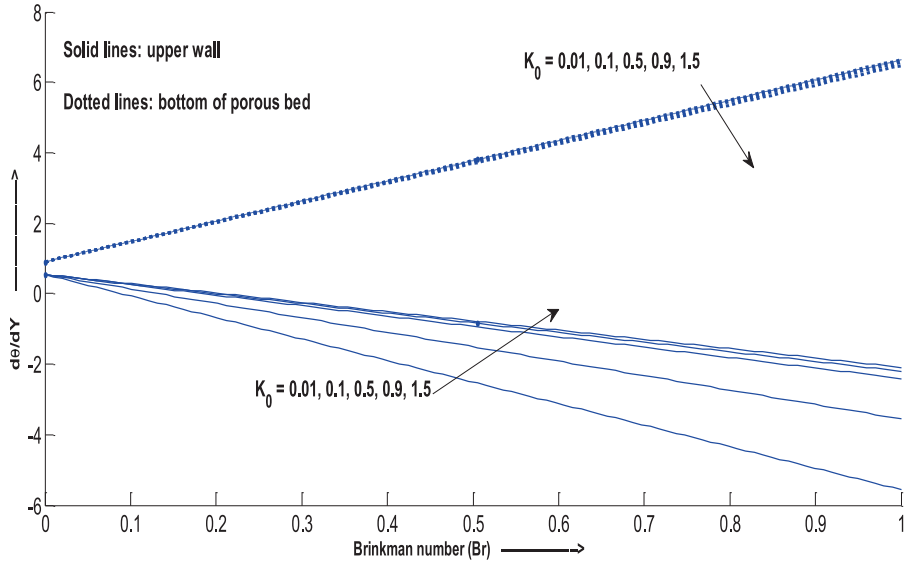

Fig. 8 (colour online). Rates of heat transfer versus Br for varying values of K_0 when $M = 1$, $C_1 = 5$, $U_0 = 5$, $A = 0.5$, $\mathrm{Nr} = 1$, $\varphi_1 = 0.8$, and $\varphi_2 = 0.6$.

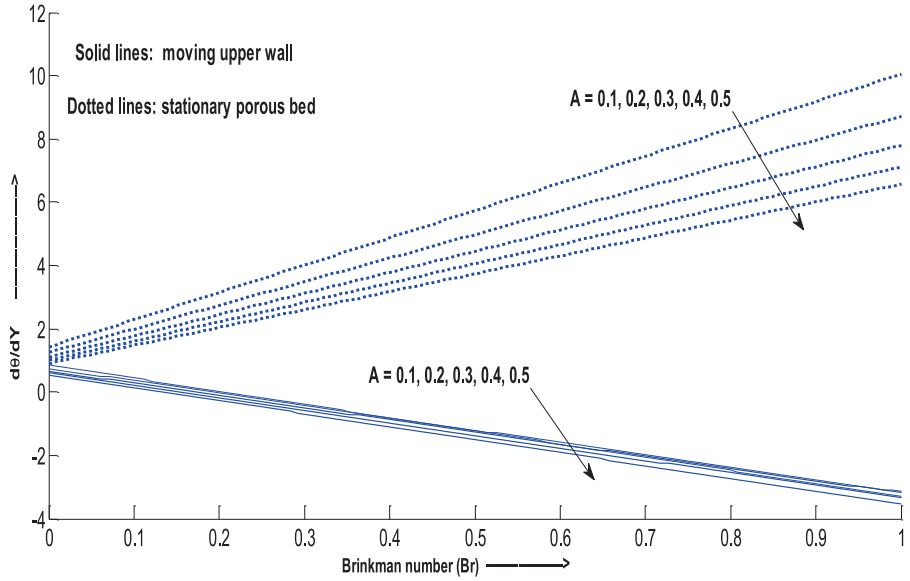

Fig. 9 (colour online). Rates of heat transfer versus Br for varying thickness A of the porous region when $M = 1$, $K_0 = 0.1$, $C_1 = 5$, $U_0 = 5$, $\mathrm{Nr} = 1$, $\varphi_1 = 0.8$, and $\varphi_2 = 0.6$.

of Br. This figure also reveals that with the increasing values of the permeability parameter K_0, $\mathrm{d}\theta/\mathrm{d}Y$ at the upper plate increases whereas it decreases at the bottom of the porous bed.

Figure 9 demonstrates the effect of the thickness of the porous layer A on the rate of heat transfer. The figure reveals that with the increasing values of A, the temperature gradient $\mathrm{d}\theta/\mathrm{d}Y$ at the upper plate decreases numerically and the same phenomenon is observed at the bottom of the porous layer.

Figure 10a and b display the effect of the magnetic field parameter M on the rates of heat transfer for the cases when $M < 1$ and $M \geq 1$, respectively. Figure 10a shows that the temperature gradient $\mathrm{d}\theta/\mathrm{d}Y$ at the bottom of the porous layer increases considerably with the increasing values of M

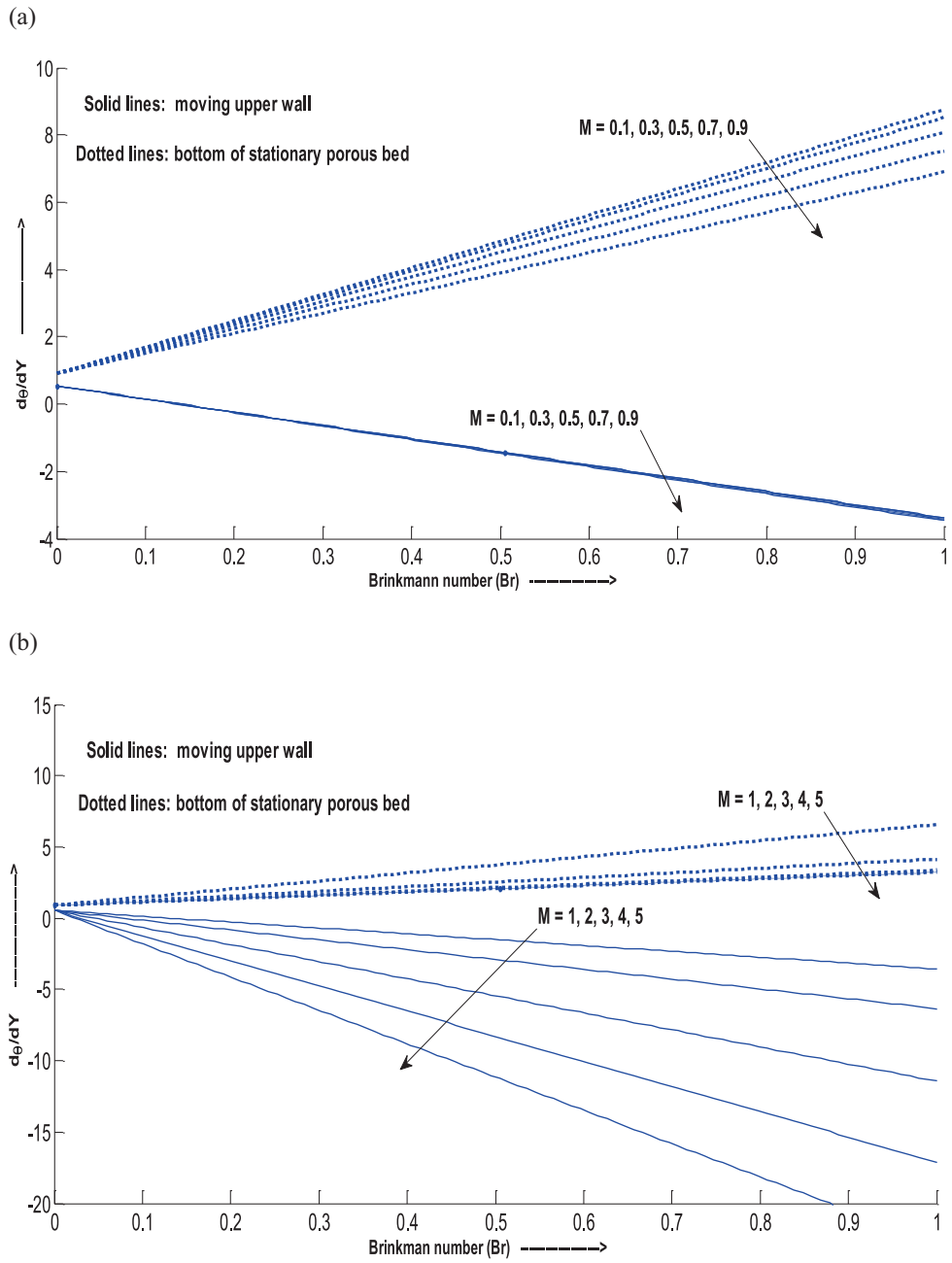

Fig. 10 (colour online). (a) Rates of heat transfer versus Br for varying M when $M < 1$ and $K_0 = 0.1$, $C_1 = 5$, $U_0 = 5$, $A = 0.5$, $\mathrm{Nr} = 1$, $\varphi_1 = 0.8$, and $\varphi_2 = 0.6$. (b) Rates of heat transfer versus Br for varying M when $M \geq 1$, $K_0 = 0.1$, $C_1 = 5$, $U_0 = 5$, $A = 0.5$, $\mathrm{Nr} = 1$, $\varphi_1 = 0.8$, and $\varphi_2 = 0.6$.

(when $M < 1$) whereas the effect of variable values of M has insignificant impact on $\mathrm{d}\theta/\mathrm{d}Y$ at the upper moving plate. In contrast to this, the impact of Hartmann number M is drastically changed for the representative values of $M \geq 1$ as is evident in Figure 10b. This figure shows that with an increase in M there is a considerable decrement in $\mathrm{d}\theta/\mathrm{d}Y$ at the moving upper wall whereas $\mathrm{d}\theta/\mathrm{d}Y$ at the bottom of

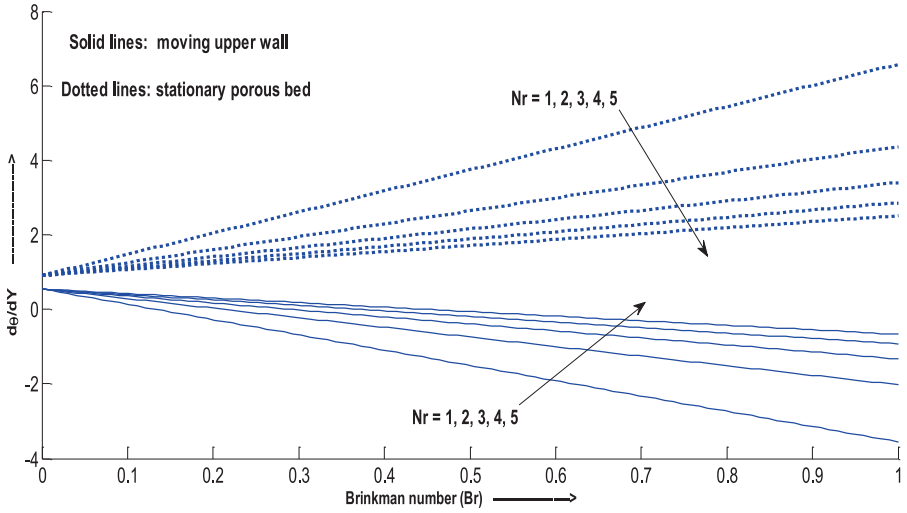

Fig. 11 (colour online). Rates of heat transfer versus Br for varying Nr when $M = 1$, $K_0 = 0.1$, $C_1 = 5$, $U_0 = 5$, $A = 0.5$, Nr = 1, $\varphi_1 = 0.8$, and $\varphi_2 = 0.6$.

the porous layer decreases very moderately with the increasing values of M.

Figure 11 depicts the effect of the radiation parameter Nr on the rate of heat transfer. The figure reveals that $\mathrm{d}\theta/\mathrm{d}Y$ at the upper plate increases considerably with the increasing values of Nr whereas it decreases at the bottom of the porous layer with increasing values of Nr.

The critical Brinkman number $\mathrm{C_{Br}}$ is that value of the Brinkman number Br at which the rate of heat transfer changes its direction. As the upper wall is at a higher temperature, hence $\mathrm{C_{Br}}$ has been calculated for the upper wall. The variation of $\mathrm{C_{Br}}$ at the upper wall with other parameters is shown in Tables 1, 2, and 3.

It is clearly visible from Table 1 that $\mathrm{C_{Br}}$ increases with increasing values of Hartmann number M up to a certain value of M say m. As M further increases (beyond m), $\mathrm{C_{Br}}$ decreases. When the velocity of the upper moving wall U_0 is low, i. e. $U_0 = 1$, then $m \cong 2.6$. But as we increase the velocity of the upper moving wall, i. e. when $U_0 = 5$, then $m \cong 0.6$.

As shown below, Table 2 clearly depicts that the critical Brinkman number $\mathrm{C_{Br}}$ increases with increasing values of the permeability parameter K_0 except for the case when the velocity of the upper moving wall U_0 is low and Hartmann number $M \leq 1$. When $U_0 = 1$ and $M \leq 1$, a reverse phenomenon is observed, i. e. $\mathrm{C_{Br}}$ decreases with increasing values of K_0. The variation of $\mathrm{C_{Br}}$ with the velocity of the upper moving wall U_0, the width of the porous layer A, and the radiation parameter Nr is shown in Table 3. It is clearly visible from it that keeping the other parameters constant, $\mathrm{C_{Br}}$ decreases on increasing A and decreasing Nr. The same phenomena occurs at $U_0 = 1$ as well as $U_0 = 5$.

5. Conclusions

The dissipative MHD Couette flow in a composite parallel plate channel partially filled with a radiating clear fluid and partially with a fluid saturated porous medium is considered. The radiative heat flux in the energy equation is assumed to follow the Rosseland approximation. The momentum and thermal energy equations have closed form solutions. They are solved using MATLAB and the solutions are obtained numerically. These solutions are analyzed in the form of graphs (Figs. 2 – 11) and tables (Tabs. 1 – 3). These results can be summarized as:

(I) On increasing the thickness of the porous layer,

1. the velocity and the temperature of the fluid increases in both regions under consideration,
2. the rates of heat transfer at the upper moving wall as well as at the bottom of the porous bed decreases, and
3. the critical Brinkman number at the upper wall decreases.

(II) As the permeability parameter increases,

1. the temperature (in both regions) decreases,
2. the rates of heat transfer at the upper wall and at the impermeable bottom decreases,

3. the critical Brinkman number at the upper plate increases except for the case when the velocity of the upper moving wall is low and the Hartmann number is ≤ 1; a reverse phenomenon is observed here, i. e. the critical Brinkman number decreases with increasing values of the permeability parameter.

(III) The effect of the Hartmann number on the thermal regime is somewhat peculiar for the two cases:

a) For low values of Hartmann number ($M \leq 1$), on increasing M

1. the temperature of the fluid decreases in both regions.
2. the rate of heat transfer increases considerably at the bottom of the porous layer while moderate impact is observed on the rate of heat transfer at the upper moving wall.

b) For high values of Hartmann number ($M \geq 1$), on increasing M

1. the temperature of the fluid in the porous region
2. and its vicinity decreases while in the clear fluid region the temperature increases considerably and has a parabolic distribution.
3. with increase in Hartmann number M there is a considerable decrement in $\mathrm{d}\theta/\mathrm{d}Y$ at the moving upper wall whereas $\mathrm{d}\theta/\mathrm{d}Y$ at the bottom of the porous layer decreases very moderately with the increasing values of M.
4. the critical Brinkman number at the upper wall increases till the Hartmann number M increases to a critical value m and decreases thereafter even on increasing M. The value of m decreases with an increase in the velocity of the upper moving plate.

(IV) On increasing Brinkman number,

1. the temperature of the fluid in both regions increases,
2. the rate of heat transfer at the upper wall decreases and the rate of heat transfer at the lower wall increases.

(V) When the radiation parameter increases,

1. the temperature of the fluid in both regions decreases,
2. the rate of heat transfer at the upper wall increases, the rate of heat transfer at the lower porous bed decreases,
3. and the critical Brinkman number at the upper wall increases.

[1] S. K. Bhargava and N. C. Sacheti, Indian J. Technol. **27**, 211 (1989).
[2] D. S. Chauhan and P. Vyas, ASCE J. Eng. Mech. **121**, 57 (1995).
[3] J. Daskalakis, Int. J. Energy. Res. **14**, 21 (1990).
[4] A. Nakayama, ASME J. Fluids Eng. **114**, 642 (1992).
[5] A. K. Al-Hadhrami, L Elliott, and D. B. Ingham, Transp. Porous Media **49**, 265 (2002).
[6] A. Pantokratoras, J. Porous Media **10**, 409 (2007).
[7] O. A. Beg, H. S. Takhar, A. J. Zueco, A. Sajid, and R. Bhargava, Acta Mech. **200**, 129 (2008).
[8] K. Vafai and S. J. Kim, J. Heat Trans. **112**, 700 (1990).
[9] P. C. Huang and K. Vafai, ASME J. Heat Trans. **116**, 768 (1994).
[10] P. C. Huang and K. Vafai, AIAA J. Thermophys. Heat Trans. **8**, 563 (1994).
[11] M. Kaviany, Int. J. Heat Mass Trans. **28**, 851 (1985).
[12] M. Kaviany, Principles of Heat Transfer in Porous Media, Springer, New York 1991.
[13] D. A. Nield and A. V. Kuznetsov, Int. J. Heat Mass Trans. **42**, 3245 (1999).
[14] K. Hooman, H. Gurgenci, and A. A. Merrikh, Int. J. Heat Mass Trans. **50**, 2051 (2007).
[15] I. G.Baoku, C. I.-Cookey, and B. I. Olajuwon, Surv. Math. Appl. **5**, 215 (2010).
[16] M. Sahraoui and M. Kaviany, Int. J. Heat Mass Trans. **35**, 927 (1992).
[17] A. V. Kuznetsov, Appli. Sci. Res. **56**, 53 (1996).
[18] A. V. Kuznetsov, Int. J. Heat Mass Trans. **41**, 2556 (1998).
[19] A. V. Kuznetsov, Acta Mech. **140**, 163 (2000).
[20] M. K. Alkam, M. A. Al-Nimr, and M. O. Hamdan, Heat Mass Trans. **38**, 337 (2002).
[21] M. A. Al-Nimr and A. F. Khadrawi, Trans. Porous Media **51**, 157 (2003).
[22] D. S. Chauhan and P. Rastogi, Turk. J. Eng. Environ. Sci. **33**, 167 (2009).
[23] D. S. Chauhan and P. Rastogi, Appl. Math. Sci. **4**, 643 (2010).
[24] G. Komurgoz, A. Arkoglu, E. Turker, and I. Ozkal, Numer. Heat Trans. Part A **57**, 603 (2010).
[25] D. S. Chauhan and R. Agrawal, Chem. Eng. Commun. **197**, 830 (2010).
[26] D. S. Chauhan and R. Agrawal, Appl. Sci. Eng. **15**, 1 (2012).
[27] M. L. Kaurangini and B. K. Jha, Appl. Math. Mech. **32**, 23 (2011).
[28] G. S. Beavers and D. D. Joseph, J. Fluid Mech. **30**, 197 (1967).
[29] G. Neale and W. Nader, Can. J. Chem. Eng. **52**, 475 (1974).
[30] S. Kim and W. B. Russel, J. Fluid Mech. **154**, 269 (1985).

[31] K. Vafai and R. Thiyagaraja, Int. J. Heat Mass Trans. **30**, 1391 (1987).
[32] J. A. Ochoa-Tapia and S. Whitakar, Int. J. Heat Mass Trans. **38**, 2635 (1995).
[33] J. A. Ochoa-Tapia and S. Whitakar, Int. J. Heat Mass Trans. **38**, 2647 (1995).
[34] B. Alazami and K. Vafai, Int. J. Heat Mass Trans. **44**, 1735 (2001).
[35] A. K. Al-Hadhrami, D. B. Elliot, and D. B. Ingham, Transp. Porous Media **53**, 117 (2003).
[36] O. A. Plumb, J. S. Huenfeld, and E. J. Eschbach, AIAA 16th Thermophysics Conference, June 23-25, Palo Alto 1981.
[37] P. Vyas and N. Srivastava, Appl. Math. Sci. **4**, 2475 (2010).
[38] P. Vyas and N. Srivastava, J. Appl. Fluid Mech. **5**, 23 (2012).
[39] P. Vyas and N. Srivastava, ISRN Thermodynamics, Article ID 214362, 9 pages, doi:10.5402/2012/214362, 2012 (2012).
[40] P. Vyas and A. Ranjan, Appl. Math. Sci. **4**, 3133 (2010).
[41] P. Vyas and A. Rai, Int. J. Contemp. Math. Sci. **5**, 2685 (2010).
[42] P. Vyas and A. Rai, Appl. Math. Sci. **6**, 4307 (2012).
[43] I. Pop, A. Ishak, and F. Aman, Z. Angew. Math. Phys. **62**, 953 (2011).
[44] T. Hayat, S. A. Shehzad, M. Qasim, and A. Alsaedi, Z. Naturforsch. **67a**, 153 (2012).
[45] M. Q. Brewster, Thermal Radiative Transfer and Properties, John Wiley and Sons, New York 1992.
[46] M. F. Modest, Heat Transfer, second edition, Academic Press, New York 2003.